NANO LETTERS

2007
Vol. 7, No. 10
3092−3096

Strain Tuning of the Photocurrent Spectrum in Single-Wall Carbon Nanotubes

Prasanth Gopinath, Aditya Mohite, Hemant Shah, Ji-Tzuoh Lin, and Bruce W. Alphenaar*

Department of Electrical and Computer Engineering, University of Louisville, Louisville, Kentucky 40292

Received July 2, 2007; Revised Manuscript Received September 12, 2007

ABSTRACT

The effect of uniaxial strain on the photocurrent spectrum of semiconducting single-wall carbon nanotubes is measured. The energy of the lowest-lying free electron transition is observed to shift with strain as predicted by a simple noninteracting model. The higher-order transitions also shift with strain, but being excitonic, their strain dependence differs from the predictions for the free carrier states. An anomalous photocurrent increase is also observed near the ground-state transition and is attributed to the formation of optically active defect states within the nanotube band gap.

The electronic structure of a single-wall nanotube (SWNT) can be substantially altered by the application of strain along the nanotube axis (uniaxial strain). Tensile strain increases the spacing between nearest-neighboring carbon atoms in the hexagonal lattice and modulates the nanotube bandstructure.[1] The energy spacing between the various bands can either increase or decrease with increasing strain depending on the nanotube chirality. Strain can also open up an energy gap in metallic nanotubes[2] or create midgap states due to defect formation.[3] A probe of the strain-dependent band structure provides insight into the nanotube electronic structure and allows for identification of the nanotube chirality. Because strain-dependent changes in carbon nanotube properties are extremely large, nanotubes can also function as strain sensors having a gauge factor of 1000% or more.[4]

While there is a great deal of information contained in the strain-dependent nanotube electronic spectrum, experiments published so far probe only the influence of strain on the lowest-lying band-to-band transition. Electrical measurements show a large change in nanotube conductance with strain,[5] while optical measurements use the amplitude of the Raman signal to show that the SWNT absorption efficiency near the band gap changes with increasing strain.[6] Recently, photoluminescence experiments show a shift in the low-energy emission of a SWNT with the application of strain.[7] These changes have been attributed to an increase or decrease in the band gap, or lowest-energy electronic transition of the carbon nanotube. No experimental studies have been published on the effect of strain on the SWNT photoexcitation spectrum over a broad energy range.

In this paper, we use a recently developed displacement photocurrent spectroscopy technique to study the influence of strain on the SWNT photoexcitation spectrum in the energy range of 0.5−3 eV. This allows us to compare the influence of strain on the lowest- and higher-order optical transitions (E_{11}, E_{22}, and E_{33}) of semiconducting SWNTs. As predicted by a simple noninteracting electron model, we observe an energy shift of each of the transitions with increasing strain, however, the sign and magnitude of the shift is generally not the same for the higher-order optical transitions as for the ground-state transition. By comparing our strain-dependent photocurrent spectrum with theory, we identify the dominant chirality of the carbon nanotubes under test. Finally, we show that the photocurrent near the lower-energy E_{11} transition shows an anomalous increase in magnitude, which we attribute to reversible strain-induced defect states opening up within the band gap.

Figure 1a shows our measurement setup. We use a previously reported displacement photocurrent technique[8−10] in which the SWNTs acts as one plate of a parallel plate capacitor. SWNTs are grown by methane-based chemical vapor deposition on a quartz slide 280 μm thick, 25.4 mm long, and 6.35 mm wide. Atomic force microscopy shows that the nanotube diameters range between 1.1 and 1.4 nm, with a tube concentration of approximately 10−15 SWNTs in a 25 × 25 sq μm area. A 25 nm thick layer of ITO is deposited by electron beam evaporation to form a transparent conducting top contact to the nanotubes, while the back of

* Corresponding author. E-mail: brucea@louisville.edu. Telephone: 502-852-1554. Fax: 502-852-8128.

10.1021/nl071582m CCC: $37.00
Published on Web 09/21/2007

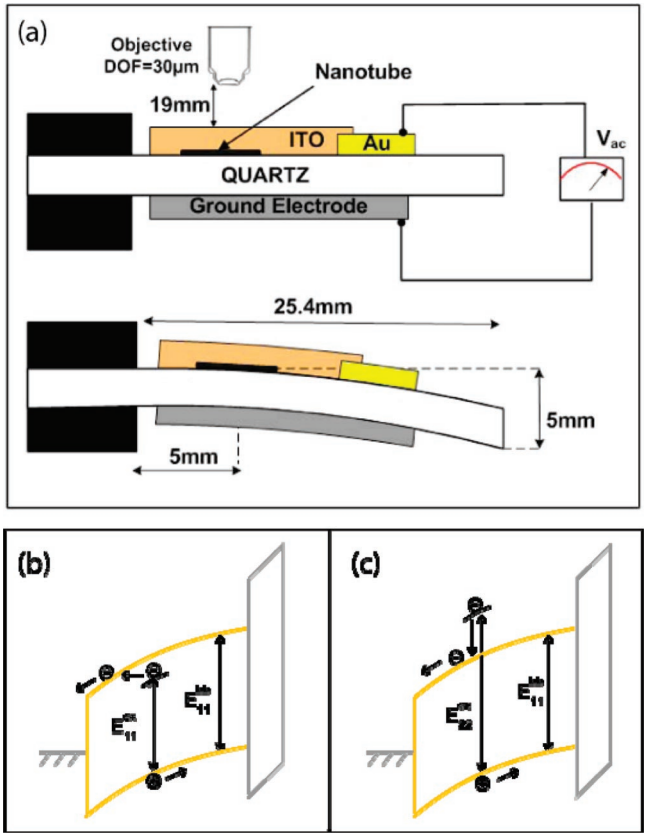

Figure 1. (a) Diagram illustrating the test device structure. The SWNTs lie parallel to sample surface. The displacement photocurrent is measured by amplifying the out of phase signal generated by the pulsed laser between the top SWNT/ITO electrode and the bottom ground electrode. The nanotubes are strained by pushing down on the free end of the quartz cantilever. (b,c) Band diagrams illustrating the photocurrent generation mechanisms for excitonic transitions (b) below and (c) above the band gap energy.

the quartz slide is coated with a conducting layer of silver epoxy to form the ground electrode. Pulsed laser light incident on the sample surface generates electron−hole pairs in the SWNTs, which redistribute to create an ac voltage across the sample. This signal can then be measured using a lock-in amplifier referenced to the laser repetition rate (1 kHz). Our optical source is a Spectra Physics optical parametric amplifier (OPA), tunable between 0.4 and 4 eV, and the output power is kept constant at 20 mW. The laser is focused on the sample surface using a microscope objective with a focal length of 20 mm and a DOF of 30 μm.

The quartz slide is loaded into an evacuated chamber and anchored at one end to form a flexible cantilever. The SWNTs are strained by pushing down on the free end of the cantilever using a probe tip, whose height can be controlled by a micrometer gauge. The amount of strain acting on the focus point (located near the base of the cantilever) is calibrated using a commercially available strain gauge. We measure a strain of 100 microstrains for a vertical displacement of 5 mm. Because the single-wall nanotubes experience a strong adhesive force to the substrate,[11] a large percentage of the strain placed on the cantilever is transferred to the nanotubes. AFM analysis shows that the SWNT's are well conformed to the cantilever surface. Because the cantilever is displaced vertically, and not twisted, the torsional strain on the SWNTs should be small. Also, because the incident laser is linearly polarized along the length of the cantilever, the contribution to the photocurrent signal will be preferentially from nanotubes that undergo uniaxial strain.

The carrier-generation mechanism in the SWNTs can be understood using the band diagrams shown in Figure 1b,c.[8] E_{11}^{bb} represents the lowest-lying free carrier (or band-to-band) transition, while E_{11}^{ex} and E_{22}^{ex} represent the two lowest-lying optically active excitonic transitions for an individual SWNT within the ITO/SWNT/dielectric capacitor. Photon absorption by the nanotube results in the excitation of an electron from the ground state to form an electron−hole pair. If the excited carriers are free, the electrons and holes will separate due to the built-in interface potential and a measurable displacement current will flow across the capacitor. If the excited carriers form excitons, then a displacement current will flow only if the bound carriers dissociate. For the E_{11}^{ex} exciton transition, which is below the band gap energy, dissociation occurs by tunneling into neighboring states (as shown in Figure 1b), and for the E_{22}^{ex} transition and other excitonic transitions, which are above the band gap energy, dissociation occurs by decay into an available lower-energy free carrier state (as shown in Figure 1c). The tunneling process is strongly field-dependent, while the decay process is relatively independent of field.

We have performed zero bias measurements of the three lowest-energy semiconductor optical transitions as a function of strain on the sample: E_{11} (0.6−0.8 eV), E_{22} (1.0−1.4 eV), and E_{33} (2.0−2.4 eV). Figure 2a shows the displacement photocurrent spectra in the E_{11} energy regime for increasing values of strain. In this case, a peak in photocurrent is observed at 0.71 eV at zero strain, and the peak shifts to lower energies with increasing strain. This is accompanied by an increase in magnitude of the background photocurrent. The peak shifts by 95 meV for 100 microstrains on the cantilever, and the magnitude of the background photocurrent increases by 400% when the cantilever is strained by 0.01%. Figure 3a shows the corresponding displacement photocurrent spectra in the E_{22} energy regime for increasing strain values up to a maximum strain value of 100 microstrains. The displacement photocurrent spectra at zero strain shows a single dominant peak at excitation energy of 1.12 eV, and the position of this peak shifts by 135 meV for 100 microstrains on the cantilever. In contrast to the E_{11} transition, no appreciable change in the background photocurrent is observed for this transition. The magnitude of the peak reduces by 4.65% when the cantilever is strained by 0.0025% and remains unchanged for higher values of strain up to 0.01%. Figure 3b shows the displacement photocurrent spectra in the E_{33} energy regime for zero strain (solid line) and for 0.01% strain (dashed line). The photocurrent peak in this energy regime is observed at 2.37 eV for zero strain, and shifts to lower energy by 45 meV when the cantilever is strained by 0.01%. This is accompanied by a reduction in magnitude of the photocurrent peak by 13.5%. The background photocurrent does not change significantly with strain in this energy regime.

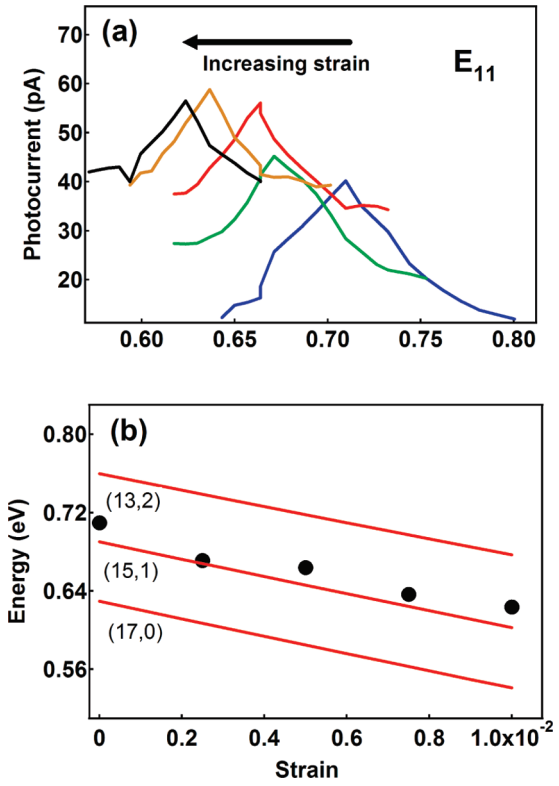

Figure 2. (a) Displacement photocurrent spectra in the E_{11} energy regime measured for a series of strain values from zero up to 100 microstrains. (b) The photocurrent peak positions plotted as a function of strain (dots), together with the lowest-lying free carrier transition energy calculated using the tight-binding model for the (13,2), (15,1) and (17,0) SWNTs. The overlap integral t_0 is taken to be 2.9.

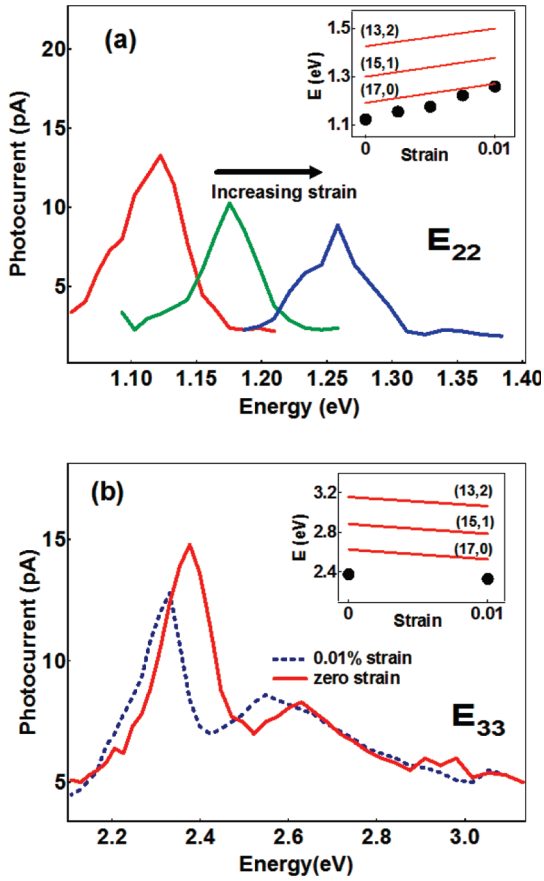

Figure 3. Displacement photocurrent spectra in the (a) E_{22} energy regime and (b) E_{33} energy regime measured for a series of strain values from zero up to 100 microstrains. The insets show the photocurrent peak positions plotted as a function of strain (dots), together with the E_{22} and E_{33} free carrier transition energies calculated using the tight-binding model for (13,2), (15,1), and (17,0) SWNTs.

As described in a previous publication,[8] the only observable photocurrent peak in the E_{11} energy regime at zero dc bias corresponds to excitation across the lowest-energy free carrier band-to-band transition. (The photocurrent corresponding to the lowest energy excitonic transition is strongly field-dependent and is only detectable if a dc bias is applied across the sample to enhance the tunneling rate into neighboring states.) It should be possible then to describe the strain dependence of the observed E_{11} peak with a simple tight-binding model, which ignores electron−electron interactions.[1] According to this model, uniaxial strain on a SWNT elongates the bond vectors, causing the band-to-band transition energy to increase or decrease depending on the chirality of the nanotube. Figure 4 plots the predicted change in energy with strain of the E_{11} band-to-band transition for all (n,m) semiconductor tubes with diameters between 0.25 and 1.6 nm. The strain dependence can be characterized by the difference between the index values $(n-m)$. The band gap increases with increasing strain in nanotubes where $[(n-m)$ mod 3] is an odd number, and the band gap decreases with increasing strain in nanotubes where $[(n-m)$ mod 3] is an even number. Larger values of $(n-m)$ produce more strain dependence than smaller values of $(n-m)$.

Plotted in this way, it can be seen that the strain-dependent transition energy provides a clearer identification of the nanotube chirality than does the zero strain transition energy alone. Figure 2b shows the shift in position of the displacement photocurrent peak in the E_{11} energy regime plotted vs the applied strain, together with the predicted shift in position of the band gap energy calculated for (17,0), (15,1), and (13,2) tubes. The band gap change with strain of a (15,1) tube with a diameter 1.23 nm fits the experimental data well, and the diameter of this nanotube falls within the average range of diameters of the CVD-grown nanotubes estimated using AFM analysis.

The higher energy photocurrent peaks observed in the E_{22} and E_{33} regimes are almost certainly excitonic in nature. In contrast with the ground-state exciton, the higher-energy excitonic transitions are observable in the photocurrent without the application of applied bias. This is because of the lower-energy free carrier states provide a decay path for exciton dissociation. At the same time, the oscillator strength of the higher-order free carrier transitions are suppressed compared with the excitonic transitions.[12] Nevertheless, it is instructive to compare the predictions of the free carrier model to the strain dependence of the E_{22} and E_{33} peaks. As shown in the insets to Figure 3a,b, the free carrier model predicts the slope of the strain dependence reasonably well; the E_{22} transition increases with increasing strain, and the E_{33} transition decreases with increasing strain, in agreement

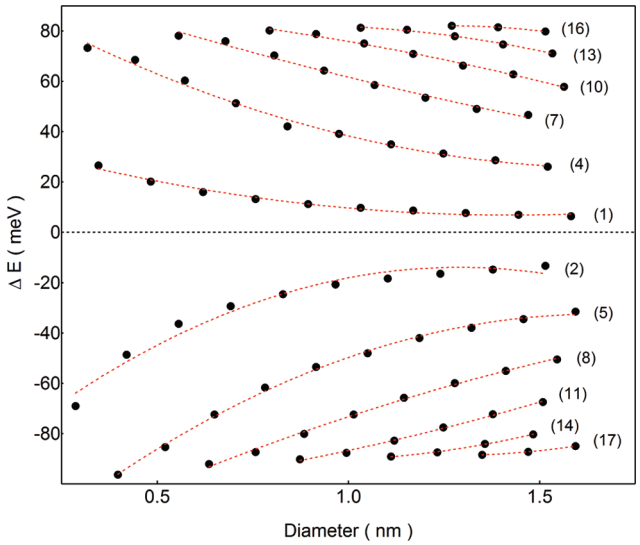

Figure 4. Change in energy with a strain of 0.01% for the E_{11} band-to-band transition calculated for all (n,m) semiconducting tubes with diameters between 0.3 and 1.6 nm. The number in brackets is the difference between the indices ($n-m$).

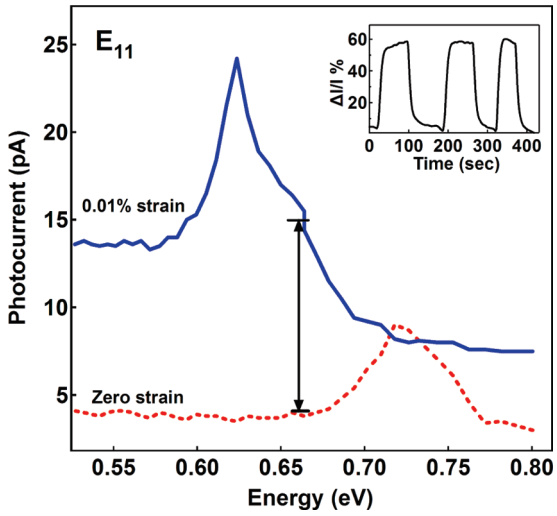

Figure 5. Displacement photocurrent in the E_{11} energy regime for zero strain (solid line) and for a strain of 0.01% (dashed line). Inset shows the change in photocurrent magnitude under repeated strains of 0.01% at fixed laser energy of 0.66 eV.

with experiment. However, the simple model overestimates the magnitude of the transition energies. This is presumably because the excitonic binding energy leads to an energy difference between the excitonic and free carrier states.

We now return to the effect of strain on the ground-state free electron transition. In this case, the peak shift with increasing strain is accompanied by a large increase in the background photocurrent. Figure 5 shows the displacement photocurrent in the E_{11} energy regime for zero strain and for a strain of 0.01%. An increase in background photocurrent is clearly seen and is most prominent in the low-energy regime. The background increase is reproducible; the inset in Figure 4 shows the percentage change in magnitude of the photocurrent for fixed laser energy of 0.66 eV under repeated strains of 0.01%, and in each case, a similar photocurrent change is observed.

The increase in background photocurrent suggests that additional states form near the free carrier band edges under strain and that these states allow for enhanced photon absorption at below band gap energies. It has been shown that structural defects in carbon nanotubes can result in the formation of additional electronic states.[3,13−15] The position of these levels with respect to the pristine carbon nanotube band structure depends on the type of defect that is formed. A common defect that forms in a nanotube under uniaxial strain is the pentagon−heptagon pair defect or the Stone−Wales transformation. It has been reported that, beyond a critical value of strain, the SWNT releases the excess strain by the spontaneous 90° rotation of a C−C bond in the hexagonal lattice, which produces a pentagon−heptagon pair.[16] The pentagon−heptagon pair defect acts as an edge dislocation in the lattice and can wrap itself around the circumference of the tube, thus creating a small section of tube with different chirality. This type of defect can strongly influence the electronic structure of the nanotube, producing pairs of donor and acceptor levels near the band edges of the nanotube.[17] The formation of these extra defect states near the band edges could possibly account for the large increase in the background photocurrent we observe with strain. We note, however, that the theoretically predicted magnitude of the critical strain required for Stone−Wales transformation to occur (>5%) is substantially higher than the strain that we are able to apply on the SWNT (0.01%) and that the Stone−Wales transformation is expected to be irreversible, in contrast with the reversible defect formation that we observe. More work is needed to account for these significant discrepancies.

In conclusion, using displacement photocurrent spectroscopy, we are able to study the effect of uniaxial strain on the optical transitions of semiconducting single-wall nanotubes. We observe a shift in the energy of the ground-state free electron transition and of the higher-order excitonic transitions with applied strain. We note that a noninteracting electron model alone does not accurately describe the magnitude and slope of the energy shift with strain for higher-order excitonic transitions. However, this model fits well with the strain dependence of the ground-state free electron transition and can be used as a unique fingerprint for assigning the chirality of carbon nanotubes. The large change in background photocurrent with strain observed for the ground-state free electron transition opens up the possibility of using carbon nanotubes as high gauge factor optical strain sensors.

Acknowledgment. We thank T. Bansal and B. Nagabhirava for their help in device fabrication and R. W. Cohn and J. Kielkopf for valuable discussions. Funding provided by ONR (no. N00014-06-1-0228) and NASA (no. NCC 5-571).

References

(1) Anantram, M. P.; Jie, H.; Lu, J. P. *Phys. Rev. B* **1999**, *60*, 13874−13878.
(2) Minot, E. D.; Yaish, Y.; Sazonova, V.; Ji-Yong, P.; Brink, M.; McEuen, P. L. *Phys. Rev. Lett.* **2003**, *90* (15), 156401.

(3) Gunn, K.; Byoung Wook, J.; Ihm, J. *Appl. Phys. Lett.* **2006**, *88*, 193107.
(4) Cao, J.; Wang, Q.; Dai, H. *Phys. Rev. Lett.* **2003**, *90*, 157601.
(5) Stampfer, C.; Jungen, A.; Linderman, R.; Obergfell, D.; Roth, S.; Hierold, C. *Nano Lett.* **2006**, *6*, 1449−1453.
(6) Cronin, S. B.; Swan, A. K.; Unlu, M. S.; Goldberg, B. B.; Dresselhaus, M. S.; Tinkham, M. *Phys. Rev. B* **2005**, *72* (3), 35425.
(7) Maki, H.; Sato, T.; Ishibashi, K. *Nano Lett.* **2007**, *7*, 890−895.
(8) Mohite, A.; Lin, J.-T.; Sumanasekera, G.; Alphenaar, B. W. *Nano Lett.* **2006**, *6*, 1369−1373.
(9) Mohite, A.; Chakraborty, S.; Gopinath, P.; Sumanasekera, G. U.; Alphenaar, B. W. *Appl. Phys. Lett.* **2005**, *86*, 061114.
(10) Vaddiraju, S.; Mohite, A.; Chin, A.; Meyyappan, M.; Sumanasekera, G.; Alphenaar, B. W.; Sunkara, M. K. *Nano Lett.* **2005**, *5*, 1625−1631.
(11) Whittaker, J. D.; Minot, E. D.; Tanenbaum, D. M.; McEuen, P. L.; Davis, R. C. *Nano Lett.* **2006**, *6*, 953−957.
(12) Perebeinos, V.; Tersoff, J.; Avouris, P. *Phys. Rev. Lett.* **2004**, *92*, 4.
(13) Choi, H. J.; Ihm, J.; Louie, S. G.; Cohen, M. L. *Phys. Rev. Lett.* **2000**, *84*, 2917−2920.
(14) Jisoon, I.; Jae-Hyeon, E.; Hoonkyung, L.; Jino, I.; Changwon, P.; Byoung Wook, J.; Seungchul, K. *Physica B* **2006**, *376*−*377*, 7−10.
(15) Charlier, J. C.; Ebbesen, T. W.; Lambin, P. *Phys. Rev. B* **1996**, *53* (16), 11108−11113.
(16) Nardelli, M. B.; Yakobson, B. I.; Bernhole, J. *Phys. Rev. B* **1998**, *57*, 4277−4280.
(17) Sungjun, L.; Gunn, K.; Hajin, K.; Byoung-Young, C.; Jhinhwan, L.; Byoung, Wook, J.; Ihm, J.; Young, K.; Se-Jong, K. *Phys. Rev. Lett.* **2005**, *95*, 166402.

NL071582M